

How Robust is the $N = 34$ Subshell Closure? First Spectroscopy of ^{52}Ar

H. N. Liu,^{1,2,3,*} A. Obertelli,^{2,1,4} P. Doornenbal,⁴ C. A. Bertulani,^{5,2} G. Hagen,^{6,7} J. D. Holt,⁸ G. R. Jansen,^{9,6} T. D. Morris,^{6,7} A. Schwenk,^{2,10,11} R. Stroberg,⁸ N. Achouri,¹² H. Baba,⁴ F. Browne,⁴ D. Calvet,¹ F. Château,¹ S. Chen,^{13,4,14} N. Chiga,⁴ A. Corsi,¹ M. L. Cortés,⁴ A. Delbart,¹ J.-M. Gheller,¹ A. Giganon,¹ A. Gillibert,¹ C. Hilaire,¹ T. Isobe,⁴ T. Kobayashi,¹⁵ Y. Kubota,^{4,16} V. Lapoux,¹ T. Motobayashi,⁴ I. Murray,^{12,4} H. Otsu,⁴ V. Panin,⁴ N. Paul,¹ W. Rodriguez,^{17,4} H. Sakurai,^{4,18} M. Sasano,⁴ D. Steppenbeck,⁴ L. Stuhl,¹⁶ Y. L. Sun,^{1,2} Y. Togano,¹⁹ T. Uesaka,⁴ K. Wimmer,¹⁸ K. Yoneda,⁴ O. Aktas,³ T. Aumann,² L. X. Chung,²⁰ F. Flavigny,¹² S. Franchoo,¹² I. Gašparić,^{21,4} R. -B. Gerst,²² J. Gibelin,²³ K. I. Hahn,²⁴ D. Kim,^{24,4} T. Koiwai,¹⁸ Y. Kondo,²⁵ P. Koseoglou,^{2,10} J. Lee,¹⁴ C. Lehr,² B. D. Linh,²⁰ T. Lokotko,¹⁴ M. MacCormick,¹² K. Moschner,²² T. Nakamura,²⁵ S. Y. Park,^{24,4} D. Rossi,² E. Sahin,²⁶ D. Sohler,²⁷ P.-A. Söderström,² S. Takeuchi,²⁵ H. Törnqvist,¹⁰ V. Vaquero,²⁸ V. Wagner,² S. Wang,²⁹ V. Werner,² X. Xu,¹⁴ H. Yamada,²⁵ D. Yan,²⁹ Z. Yang,⁴ M. Yasuda,²⁵ and L. Zanetti²

¹IRFU, CEA, Université Paris-Saclay, F-91191 Gif-sur-Yvette, France

²Institut für Kernphysik, Technische Universität Darmstadt, 64289 Darmstadt, Germany

³Department of Physics, Royal Institute of Technology, SE-10691 Stockholm, Sweden

⁴RIKEN Nishina Center, 2-1 Hirosawa, Wako, Saitama 351-0198, Japan

⁵Texas A&M University-Commerce, PO Box 3011, Commerce, Texas 75429, USA

⁶Physics Division, Oak Ridge National Laboratory, Oak Ridge, Tennessee 37831, USA

⁷Department of Physics and Astronomy, University of Tennessee, Knoxville, Tennessee 37996, USA

⁸TRIUMF 4004 Wesbrook Mall, Vancouver, British Columbia V6T 2A3, Canada

⁹National Center for Computational Sciences, Oak Ridge National Laboratory, Oak Ridge, Tennessee 37831, USA

¹⁰ExtreMe Matter Institute EMMI, GSI Helmholtzzentrum für Schwerionenforschung GmbH, 64291 Darmstadt, Germany

¹¹Max-Planck-Institut für Kernphysik, Saupfercheckweg 1, 69117 Heidelberg, Germany

¹²Institut de Physique Nucléaire, CNRS-IN2P3, Université Paris-Sud, Université Paris-Saclay, 91406 Orsay Cedex, France

¹³State Key Laboratory of Nuclear Physics and Technology, Peking University, Beijing 100871, P.R. China

¹⁴Department of Physics, The University of Hong Kong, Pokfulam, Hong Kong

¹⁵Department of Physics, Tohoku University, Sendai 980-8578, Japan

¹⁶Center for Nuclear Study, University of Tokyo, RIKEN campus, Wako, Saitama 351-0198, Japan

¹⁷Universidad Nacional de Colombia, Sede Bogotá, Facultad de Ciencias, Departamento de Física, 111321, Bogotá, Colombia

¹⁸Department of Physics, University of Tokyo, 7-3-1 Hongo, Bunkyo, Tokyo 113-0033, Japan

¹⁹Department of Physics, Rikkyo University, 3-34-1 Nishi-Ikebukuro, Toshima, Tokyo 172-8501, Japan

²⁰Institute for Nuclear Science & Technology, VINATOM, P.O.Box 5T-160, Nghia Do, Hanoi, Vietnam

²¹Ruder Bošković Institute, Zagreb, Croatia

²²Institut für Kernphysik, Universität zu Köln, D-50937 Cologne, Germany

²³LPC Caen, ENSICAEN, Université de Caen, CNRS/IN2P3, F-14050 Caen, France

²⁴Department of Physics, Ewha Womans University, Seoul, South Korea

²⁵Department of Physics, Tokyo Institute of Technology, 2-12-1 O-Okayama, Meguro, Tokyo, 152-8551, Japan

²⁶Department of Physics, University of Oslo, N-0316 Oslo, Norway

²⁷MTA Atomki, P.O. Box 51, Debrecen H-4001, Hungary

²⁸Instituto de Estructura de la Materia, CSIC, E-28006 Madrid, Spain

²⁹Institute of Modern Physics, Chinese Academy of Sciences, Lanzhou, China

(Dated: May 6, 2022)

The first γ -ray spectroscopy of ^{52}Ar , with the neutron number $N = 34$, was measured using the $^{53}\text{K}(p,2p)$ one-proton removal reaction at ~ 210 MeV/u at the RIBF facility. The 2_1^+ excitation energy is found at 1656(18) keV, the highest among the Ar isotopes with $N > 20$. This result is the first experimental signature of the persistence of the $N = 34$ subshell closure beyond ^{54}Ca , i.e., below the magic proton number $Z = 20$. Shell-model calculations with phenomenological and chiral-effective-field-theory interactions both reproduce the measured 2_1^+ systematics of neutron-rich Ar isotopes, and support a $N = 34$ subshell closure in ^{52}Ar .

PACS numbers: xxxxxxxx

In the shell model description of atomic nuclei, magic numbers of nucleons correspond to fully occupied energy shells below the Fermi surface [1], and present the backbone of our understanding of nuclei. Scientific advances over the past decades have shown that the sequence of magic numbers established for stable nuclei—2, 8, 20, 28, 50, 82, 126—is not universal across the

nuclear landscape [2]. A few prominent examples are the breakdown of the conventional $N = 20$, 28 magic numbers [3–5] and the emergence of a new $N = 16$ magic number [6, 7] in neutron-rich nuclei. Considerable efforts have been spent to unfold the driving forces behind such shell evolution. In particular, the spin-isospin terms of the monopole part of the effective nucleon-nucleon

interactions [8, 9], as well as three-nucleon forces [10, 11] have been proposed to play a dominant role.

For rare isotopes, the first 2^+ excitation energy [$E(2_1^+)$] in even-even nuclei is often the first observable accessible to experiment to characterize shell effects. In a simplified shell model picture, a high 2_1^+ excitation energy is interpreted as resulting from the excitation of nucleons across a large shell gap [12].

Recently, neutron-rich pf -shell nuclei have received much attention on both experimental and theoretical fronts with the possible appearance of new subshell closures at $N = 32$ and 34 . A sizable $N = 32$ subshell closure has been reported in the region from Ar to Cr isotopes based on $E(2_1^+)$ [13–16], reduced transition probabilities $B(E2; 0_1^+ \rightarrow 2_1^+)$ [17, 18], and mass [19–21] measurements, although some ambiguity remains due to the newly measured large charge radii of neutron-rich Ca isotopes [22], the masses of $^{51-55}\text{Ti}$ [23], and the low $E(2_1^+)$ in ^{50}Ar [16]. On the other hand, the $N = 34$ subshell closure has been so far suggested only in ^{54}Ca [24, 25]. In the Ti and Cr isotopes, the systematics of $E(2_1^+)$ [26, 27] and $B(E2; 0_1^+ \rightarrow 2_1^+)$ [17, 18] show no local maximum and minimum at $N = 34$. The measured low-lying structure of ^{55}Sc [28] was interpreted as indicating a rapid weakening of the $N = 34$ subshell closure in pf -shell nuclei at atomic number $Z > 20$. The $E(2_1^+)$ of ^{54}Ca was measured to be 2043(19) keV, ~ 0.5 MeV lower than its even-even neighbor ^{52}Ca [24]. Despite this lower 2_1^+ excitation energy, ^{54}Ca was concluded to be a doubly magic nucleus from a phenomenological shell-model interpretation [24], whereas *ab initio* coupled-cluster calculations indicated a weak $N = 34$ subshell closure [29]. Very recently, the mass measurements of $^{55-57}\text{Ca}$ [25] confirmed the picture of a subshell closure at $N = 34$ in Ca isotopes. Until now, the region below $Z = 20$ was unexplored. It is still an open question how the $N = 34$ subshell evolves below $Z = 20$ towards more neutron-rich systems, such as ^{52}Ar .

The heaviest Ar isotope with known spectroscopic information so far is ^{50}Ar [16]. Phenomenological shell-model calculations [24, 30] reproducing the available $E(2_1^+)$ data for neutron-rich Ar isotopes predict a relatively high-lying 2_1^+ state in ^{52}Ar , and suggest that the $N = 34$ subshell closure in ^{52}Ar is stronger than the one reported for ^{54}Ca [16]. In the present Letter, we report on the first spectroscopy of ^{52}Ar , the most neutron-rich even-even $N = 34$ isotope accessible today and possibly for the next decades. A clear enhancement of $E(2_1^+)$ at $N = 34$ is found, supporting the persistence of the $N = 34$ magic number in $Z < 20$ nuclei.

The experiment was carried out at the Radioactive Isotope Beam Factory (RIBF), operated by the RIKEN Nishina Center and the Center for Nuclear Study of the University of Tokyo. Radioactive nuclei were produced by fragmentation of a 345 MeV/u ^{70}Zn primary beam with an average beam intensity of ~ 240 pnA on a 10-mm-

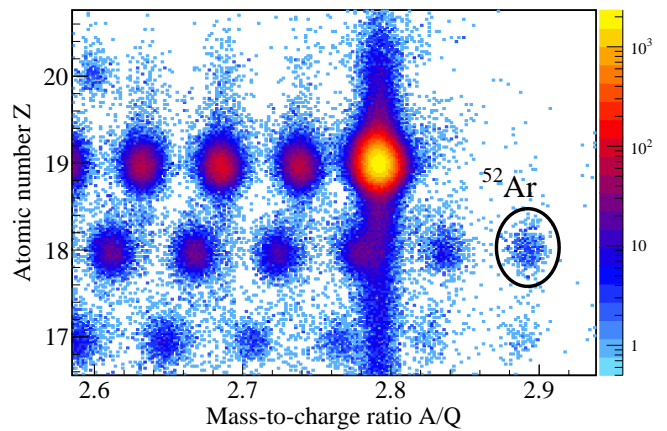


FIG. 1. (Color online) Particle identification plot of reaction residues with the selection of the incoming ^{53}K beam impinging on the secondary target.

thick rotating Be target. The secondary beam cocktail, magnetically centered on ^{53}K , was identified event-by-event using the magnetic rigidity ($B\rho$), energy loss (ΔE) and time-of-flight (TOF) information [31] in the BigRIPS two-stage fragment separator [32]. The intensity and purity of the ^{53}K beam were ~ 1.0 particle per second and $\sim 0.5\%$, respectively.

The secondary beam impinged on a 151(1)-mm-thick liquid hydrogen (LH_2) target with a density of 73 kg/m³ to induce one-proton knockout reactions. Two multiwire drift chambers [33], located upstream of the LH_2 target, were used to measure the trajectories of the incoming projectiles. The kinetic energy of the ^{53}K beam at the entrance of the target was ~ 245 MeV/u. Its energy loss in the LH_2 target was approximately 70 MeV/u. The LH_2 target was surrounded by a 300-mm-long time projection chamber (TPC), constituting the MINOS device [34]. The tracks of the recoil protons were recorded by the TPC to reconstruct the reaction vertex [35]. The MINOS efficiency to detect at least one of the two protons was measured to be 92(3)%. The vertex resolution was estimated to be 4 mm (FWHM) [35]. The determination of the reaction vertices allowed precise Doppler correction of the de-excitation γ rays from the reaction residues.

The DALI2+ [36] high-efficiency γ -ray spectrometer surrounded the MINOS device to detect in-flight de-excitation γ rays from ^{52}Ar . It consisted of 226 NaI(Tl) crystals and covered polar angles from 15° to 118° with respect to the center of the LH_2 target. Add-back analysis was applied for events with γ -ray multiplicity $M_\gamma > 1$ when the centers of hit detectors were less than 20 cm apart. For 1 MeV γ rays emitted from nuclei moving at 60% of the velocity of light, the photopeak efficiency and energy resolution after add-back analysis were 30% and 11% (FWHM), respectively. The whole array was calibrated using ^{133}Ba , ^{137}Cs , ^{60}Co , and ^{88}Y

sources leading to an energy calibration uncertainty of 4 keV, and showed a good linearity from 356 keV to 1836 keV.

Downstream the LH₂ target, reaction residues were transported to the SAMURAI spectrometer [33] and identified with the $B\rho$ - ΔE -TOF method. The $B\rho$ of charged fragments passing through the SAMURAI magnet with a central magnetic field of 2.7 T was reconstructed using two multiwire drift chambers placed upstream and downstream the magnet [33]. The ΔE and TOF information were provided by a 24-element plastic scintillator hodoscope. Figure 1 shows the particle identification of fragments with the selection of ^{53}K identified at BigRIPS. A 6.6σ separation in Z and a 9.1σ separation in mass number, A , for Ar isotopes were achieved. Over the data taking of seven days, 438 counts of ^{52}Ar were obtained from the $^{53}\text{K}(p, 2p)^{52}\text{Ar}$ reactions, in which the kinematics of protons measured by MINOS supported a quasi-free scattering reaction mechanism. The reaction loss of ^{53}K in materials along the beam and fragment trajectories was determined by measuring the unreacted ^{53}K , and the inclusive cross section was measured to be 1.9(1) mb.

The Doppler-shift corrected γ -ray energy spectrum of ^{52}Ar following the $^{53}\text{K}(p, 2p)$ reaction is shown in Fig. 2. A clear peak is present in the range of 1500-1800 keV, while three structures are visible in the range of 600-900, 1000-1300 and 2000-2500 keV. In order to quantify the significance level of these peaks, we performed the likelihood ratio test by fitting the spectrum of ^{52}Ar using the GEANT4 [37] simulated response functions on top of a double exponential background. Given the low statistics of the γ -ray spectrum of ^{52}Ar , a Poisson distribution was adopted to describe the fluctuations of each bin, and the background line shape was constrained by the measured γ -ray spectrum in coincidence with ^{50}Ar following the $^{51}\text{K}(p, 2p)$ reaction. As a result, a significance level of 5 standard deviations (σ) was obtained for the 1656(18) keV transition. The 2295(39) keV γ line was found to have a significance of 3 σ , while the other two structures in the range of 600-900 and 1000-1300 keV both had a significance level of less than 1 σ and are therefore not considered in the following analysis. Note that the errors of the deduced γ -ray energies shown above include both statistical and systematic uncertainties. The former dominates and the latter mainly originates from the energy calibration uncertainty. Lifetime (τ_γ) effects of the excited states on the deduced γ -ray energies are expected to be negligible, since Raman's global systematics [38] suggests $\tau_\gamma < 2$ ps for the two excited states measured in ^{52}Ar .

Based on the measured γ -ray intensities, the 1656 keV transition is attributed to a direct decay to the ground state. The low statistics do not allow to conclude any (non) coincidence between the 1656 and 2295 keV transitions from γ - γ correlations, but the cascade

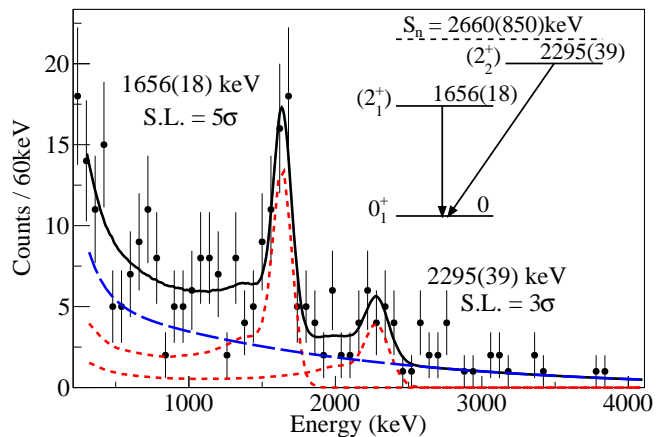


FIG. 2. (Color online) Doppler-shift corrected γ -ray energy spectrum of ^{52}Ar following the $^{53}\text{K}(p, 2p)$ reaction. The fit function to the spectrum (black solid line) includes simulated response functions for the observed transitions (red dotted line) and a double-exponential background (blue dashed line). The significance level (S.L.) is given for the observed transitions. The deduced experimental level scheme is shown in the inset. See text for details.

scenario is very unlikely due to the expected low neutron separation energy (S_n) of ^{52}Ar . The recent precision mass measurement gives $S_n = 3840(70)$ keV for ^{54}Ca [19]. Being more exotic, ^{52}Ar is expected to have a significantly lower S_n . The 2016 Atomic Mass Evaluation [39] gives an estimation $S_n = 2660(850)$ keV for ^{52}Ar , and excludes the coincidence scenario. The proposed energy level scheme of ^{52}Ar is presented in the inset of Fig. 2. The measured partial cross sections to the 1656 and 2295 keV states are 0.9(2) and 0.4(1) mb, respectively. Assuming no population to other excited states, the cross section to the ground state is deduced to be 0.7(2) mb via subtraction from the inclusive cross section. The quoted uncertainties are dominated by statistical errors, while the systematic uncertainties mainly arise from the estimation of MINOS efficiency. All the experimental results are summarized in Table I. The 1656 keV state with the higher population is assigned to be 2_1^+ . The 2295 keV state decaying directly to the ground state is assigned as 2_2^+ . Further discussions about these spin-parity assignments are given later based on the comparison between experimental partial cross sections and theoretical calculations.

Figure 3 displays the energy of the 2_1^+ state deduced for ^{52}Ar together with values for lighter Ar isotopes [40]. Notably, the measured $E(2_1^+) = 1656(18)$ keV for ^{52}Ar is found to be the highest among the Ar isotopes with $N > 20$. It is larger than the $E(2_1^+) = 1577(1)$ keV [41] for ^{46}Ar which reflects the conventional $N = 28$ shell closure. Moreover, the measured systematics of $E(2_1^+)$ along the Ar isotopic chain is characterized by a pronounced enhancement at $N = 34$ relative to its $N =$

32 even-even neighbor, unlike the trend observed for Ca, Ti and Cr isotopes in which a decrease is seen from $N = 32$ to 34. The present work offers the first experimental signature of the $N = 34$ subshell closure in Ar isotopes.

To gain further insight into the structure of ^{52}Ar , we compare our results to state-of-the-art nuclear structure calculations. Here, two advanced *ab initio* approaches are adopted: the valence-space in-medium similarity renormalization group (VS-IMSRG) [42–45] (for calculational details, see in particular Refs. [45, 46]) and coupled cluster theory [47, 48], employing two sets of two- (NN) and three-nucleon ($3N$) interactions derived from chiral effective field theory [49, 50]: 1.8/2.0(EM) [46, 51, 52] and $N^2\text{LO}_{\text{sat}}$ [53]. The coupled-cluster method is particularly well suited for closed (sub-) shell nuclei and their neighbors. By employing a double-charge exchange equation-of-motion (DCE-EOM) coupled-cluster technique, the $E(2_1^+)$ states in $^{40,48,52}\text{Ar}$ can be obtained from generalized excitations of the ground states of the closed (sub-)shell nuclei $^{40,48,52}\text{Ca}$, while the $E(2_1^+)$ state in ^{44}Ar is obtained from excitations of the ^{44}S ground state, respectively. The $E(2_1^+)$ states in $^{46,50,52}\text{Ar}$ are also computed using the two-particle-removed equation-of-motion coupled-cluster method [54] (denoted by 2PR-EOM).

In this work, we employ the DCE-EOM coupled-cluster calculations with particle-hole excitations truncated at the singles, doubles, and approximate triples level (CCSDT-3) [55], while the 2PR-EOM coupled-cluster calculations are truncated at the three-hole-one-particle excitation level using CCSD and CCSDT-3 for the ground states of $^{48,52,54}\text{Ca}$. Theoretical uncertainties in coupled-cluster calculations are estimated by comparing results with and without triples excitations. In addition, we also compare our results to large scale shell-model calculations with the phenomenological SDPF-MU effective interaction [56]. Note that the original SDPF-MU Hamiltonian was modified using recent experimental data on exotic Ca [24] and K [57] isotopes. The pf -shell part of the new interaction is the GXPF1Br Hamiltonian and details of the modifications are given in Ref. [30].

Theoretical $(p,2p)$ cross sections to different final states of ^{52}Ar are computed with spectroscopic factors calculated with the VS-IMSRG method using the 1.8/2.0 (EM) interaction and single-particle cross sections (σ_{sp}) calculated using the Glauber theory as described in Ref. [58]. The input of the σ_{sp} calculations are the nucleon-nucleon cross sections, using the parametrization from Ref. [59], and the nuclear ground-state densities deduced from a mean-field Hartree-Fock-Bogoliubov calculation using the SLy4 interaction. The involved single-particle states are calculated using a Woods-Saxon potential including the Coulomb and spin-orbit terms with parameters chosen to reproduce the proton separation energies. The range of the Woods-Saxon potential was taken as $R = r_0(A - 1)^{1/3}$ fm with $r_0 = 1.25$ fm, and the

TABLE I. Experimental excitation energies (E_{exp}) and cross sections (σ_{exp}) from the $^{53}\text{K}(p,2p)^{52}\text{Ar}$ reaction in comparison with theoretical calculations. Predicted excitation energies (E_x), J^π , and spectroscopic factors (C^2S_{th}) associated with the removed protons from different orbits (l_j) were obtained using the VS-IMSRG method predicting a $^{53}\text{K}(3/2^+)$ ground state. Theoretical partial cross sections (σ_{th}) were computed using the C^2S_{th} values and beam-energy-weighted average single-particle cross sections ($\langle\sigma_{\text{sp}}\rangle$).

Experiment		Theory					
E_{exp} (keV)	σ_{exp} (mb)	E_x (keV)	J^π	l_j	C^2S_{th}	$\langle\sigma_{\text{sp}}\rangle$ (mb)	σ_{th} (mb)
0	0.7(2) ^a	0	0_1^+	$d_{3/2}$	0.28	3.03	0.86
1656(18)	0.9(2)	1849	2_1^+	$s_{1/2}$	0.10	0.92	1.13
				$d_{3/2}$	0.33	2.94	
				$d_{5/2}$	0.02	4.82	
		1974	0_2^+	$d_{3/2}$	0.01	2.93	0.04
2295(39)	0.4(1)	2367	2_2^+	$s_{1/2}$	0.13	0.92	0.30
				$d_{3/2}$	0.05	2.91	
				$d_{5/2}$	0.01	4.76	
Inclusive	1.9(1)						2.32

^a It is deduced by assuming no population to other excited states except the 1656- and 2295-keV state. See text for details.

diffuseness is chosen as 0.65 fm. The strength of the spin-orbit potential is set to -6 MeV. Since the reaction vertices were reconstructed with MINOS, the energy dependence of the cross section was considered by taking the average of σ_{sp} at different incident energies weighted by observed statistics ($\langle\sigma_{\text{sp}}\rangle$). As an illustration, σ_{sp} for the removal of a $d_{3/2}$ proton in ^{53}K to the ground state of ^{52}Ar varies from 2.38 mb at 180 MeV/u to 3.64 mb at 246 MeV/u. Table I lists theoretical results for the states lying below the extrapolated $S_n = 2660(850)$ keV of ^{52}Ar [39]. The proton removal from three orbits contributes to the population of 2^+ state in ^{52}Ar : $s_{1/2}$, $d_{3/2}$ and $d_{5/2}$. As shown in Table I, the measured cross sections to the 1656 and 2295 keV states in ^{52}Ar agree well with the predictions for the 2_1^+ state at 1849 keV and the 2_2^+ state at 2367 keV, respectively. The ratio of the experimental cross section to the theoretical prediction is in line with the systematic reduction factor reported from $(e,e'p)$ measurements on stable targets [60] and from $(p,2p)$ reactions on oxygen isotopes [61, 62]. The good agreement between experiment and theory not only supports the spin-parity assignment, but also indicates that the adopted VS-IMSRG approach provides a satisfactory description of the structure of ^{52}Ar with the 1.8/2.0 (EM) interaction.

We now discuss the systematics of $E(2_1^+)$ in Ar isotopes. As seen in Fig. 3, the phenomenological shell-model calculations with the original and modified SDPF-MU interaction and the VS-IMSRG calculations with the 1.8/2.0 (EM) interaction reproduce the steep rise of $E(2_1^+)$ from ^{50}Ar to ^{52}Ar . The modified SDPF-MU calculations provide the best overall description of the

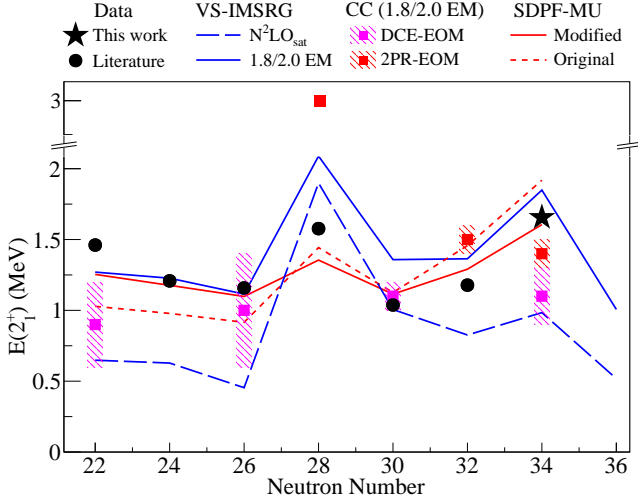


FIG. 3. (Color online) Experimental 2_1^+ energies for even-even Ar isotopes compared with theory: VS-IMSRG with the chiral interaction 1.8/2.0(EM) and $N^2\text{LO}_{\text{sat}}$, coupled-cluster calculations (CC) using the DCE-EOM and 2PR-EOM methods with the 1.8/2.0(EM) interaction, and phenomenological shell model calculations with the original and modified SDPF-MU effective interaction [16]. The hatched regions represent the theoretical uncertainties in coupled-cluster calculations. Experimental data are taken from Ref. [40] and this work. Note the broken y-axis scale between 2.2 and 2.7 MeV. See text for details.

experimental data along the Ar isotopic chain including the $E(2_1^+)$ of ^{52}Ar . The VS-IMSRG approach using the 1.8/2.0 (EM) interaction reasonably reproduces the measured $E(2_1^+)$ in neutron-rich Ar isotopes, though an overprediction is seen between $N = 28$ and 34. The dependence of the *ab initio* calculations on the initial NN and $3N$ forces is illustrated by the VS-IMSRG calculations with the $N^2\text{LO}_{\text{sat}}$ Hamiltonian. Compared to results with the 1.8/2.0 (EM) interaction, calculations with the $N^2\text{LO}_{\text{sat}}$ interaction systematically underpredict the data, despite a better agreement for the $E(2_1^+)$ at $N = 28$ and 30. The DCE-EOM calculations with the 1.8/2.0 (EM) interaction reproduce the $E(2_1^+)$ in $^{44,48}\text{Ar}$ within the estimated uncertainties, but underestimate the $E(2_1^+)$ in ^{52}Ar by ~ 600 keV. For ^{40}Ar , which is characterized by deformation and shape co-existence [63], all considered calculations underestimate its $E(2_1^+)$. The 2PR-EOM result for ^{52}Ar is consistent with the DCE-EOM result, but does not reproduce the steep increase of the $E(2_1^+)$ state from ^{50}Ar to ^{52}Ar . We note that 2PR-EOM gives a $E(2_1^+)$ energy at 3.0 MeV consistent with the $N = 28$ shell closure, although almost twice the experimental value.

Being rooted in the same chiral effective interaction, i.e., 1.8/2.0 (EM), the VS-IMSRG and coupled-cluster approaches predict different $E(2_1^+)$ in ^{52}Ar . However, for closed (sub-)shell Ca isotopes, VS-IMSRG predicts

similar $E(2_1^+)$ as coupled-cluster calculations with singles and doubles excitations (EOM-CCSD), despite they both overestimate the $E(2_1^+)$ in $^{48,52}\text{Ca}$. Compared to EOM-CCSD and VS-IMSRG, EOM-CCSDT-3 gives overall lower $E(2_1^+)$. It reproduces the measured $E(2_1^+)$ in $^{48,52}\text{Ca}$, but underestimates the $E(2_1^+)$ in ^{54}Ca by 300 keV. The differences in the calculated $E(2_1^+)$ states in calcium and argon isotopes using the employed many-body methods, indicate that the total theoretical uncertainties might be larger than the estimated error bars shown in Fig. 3. Thus, the measured $E(2_1^+)$ state of ^{52}Ar in the current work serves as an important benchmark to understand these uncertainties.

It is worth noting that the modified SDPF-MU shell model calculations and the VS-IMSRG approach using the 1.8/2.0 (EM) interaction have both been used along the $N = 34$ isotonic chain to investigate the evolution of the shell closure. Both calculations suggest that the $N = 34$ shell gap persists from ^{54}Ca towards more exotic $N = 34$ isotones, which is consistent with the measured high-lying 2_1^+ state in ^{52}Ar presented here. However, the shell gap is not an observable, so calculations predicting similar $E(2_1^+)$ might give different sizes of shell gaps. Indeed, the modified SDPF-MU calculations indicate that the magnitude of the $N = 34$ shell gap in ^{52}Ar is ~ 3.1 MeV, which exceeds the value in ^{54}Ca (~ 2.6 MeV) [16]. Conversely, using the method of Ref. [64] to extract the effective single-particle energies, VS-IMSRG predicts the $N = 34$ shell gap in ^{52}Ar to be ~ 2.6 MeV, smaller than that in ^{54}Ca (~ 3.2 MeV). In addition, the VS-IMSRG approach also provides the orbital occupancies of the 0_1^+ and 2_1^+ states in ^{52}Ar and ^{54}Ca . It reveals that only ~ 0.5 neutrons are excited from $p_{1/2}$ to $f_{5/2}$ in the 2_1^+ excitation of ^{52}Ar , whereas in the case of ^{54}Ca , ~ 0.9 neutrons are excited across the $N = 34$ shell gap. This is consistent with the observed decrease in $E(2_1^+)$ between ^{54}Ca and ^{52}Ar . Nevertheless, both calculations predict ^{48}Si as a new doubly magic nucleus. The $E(2_1^+)$ of ^{48}Si in SDPF-MU [30] and VS-IMSRG [65] calculations lies at 2.85 and 3.13 MeV, respectively. However, it is not yet known whether ^{48}Si is stable against neutron emission. Mass models that reproduce well the observed limits of existence in the pf -shell region [66] tend to predict ^{48}Si as a drip line nucleus.

To summarize, the low-lying structure of the $N = 34$ nucleus ^{52}Ar was investigated using the $^{53}\text{K}(p,2p)^{52}\text{Ar}$ one-proton removal reaction at ~ 210 MeV/u mid-target energy. The 2_1^+ state was measured to be 1656(18) keV, the highest among the Ar isotopes with $N > 20$. The measured $(p,2p)$ cross sections to different final states of ^{52}Ar are in line with calculations and support the proposed spin-parity assignment. Shell-model calculations with phenomenological and the chiral interaction 1.8/2.0 (EM) both reproduce the measured 2_1^+ systematics of the neutron-rich Ar isotopes, and suggest a $N = 34$ subshell closure in ^{52}Ar . However, the coupled-

cluster calculations based on the same chiral interaction underestimate the 2_1^+ excitations in ^{52}Ar . The measured $E(2_1^+)$ of ^{52}Ar serves as an important benchmark to understand the uncertainties of the employed many-body methods and chiral effective-field-theory interactions. Our results offer the first experimental signature of the persistence of the $N = 34$ subshell closure below $Z = 20$, and agree with shell-model calculations predicting ^{48}Si as a new doubly magic nucleus far from stability.

We thank the RIBF accelerator staff for their work in the primary beam delivery and the BigRIPS team for preparing the secondary beams. We acknowledge Y. Utsuno for providing us the SDPF-MU calculated 2_1^+ excitation energies for Ar isotopes and ^{48}Si . The development of MINOS has been supported by the European Research Council through the ERC Grant No. MINOS-258567. H. N. L. thanks G. Schnabel and R. Taniuchi for valuable discussions about the significance level estimation and acknowledges the support from the Enhanced Eurotalents program (PCOFUND-GA-2013-600382) co-funded by CEA and the European Union. H. N. L. and A. S. acknowledges the support from the Deutsche Forschungsgemeinschaft through Grant SFB 1245. C. A. B. acknowledges support from the U.S. NSF grant No. 1415656 and the U.S. DOE grant No. DE-FG02-08ER41533. Y. L. S. acknowledges the support of Marie Skłodowska-Curie Individual Fellowship (H2020-MSCA-IF-2015-705023) from the European Union. I. G. has been supported by HIC for FAIR and Croatian Science Foundation. L.X.C. and B.D.L. have been supported by the Vietnam MOST through the Physics Development Program Grant No. DTDLN.25/18. This work was also supported by the Office of Nuclear Physics, U.S. Department of Energy, under grants de-sc0018223 (NUCLEI SciDAC-4 collaboration) and the Field Work Proposal ERKBP72 at Oak Ridge National Laboratory (ORNL). Computer time was provided by the Innovative and Novel Computational Impact on Theory and Experiment (INCITE) program. This research used resources of the Oak Ridge Leadership Computing Facility located at ORNL, which is supported by the Office of Science of the Department of Energy under Contract No. DE-AC05-00OR22725.

* hliu@ikp.tu-darmstadt.de

- [1] M. Mayer and J. H. D. Jensen, *Elementary Theory of Nuclear Shell Structure* (Wiley, New York, 1955).
- [2] O. Sorlin and M.-G. Porquet, *Prog. Part. Nucl. Phys.* **61**, 602 (2008).
- [3] C. Thibault *et al.*, *Phys. Rev. C* **12**, 644 (1975).
- [4] D. Guillemaud-Mueller *et al.*, *Nucl. Phys. A* **426**, 37 (1984).
- [5] B. Bastin *et al.*, *Phys. Rev. Lett.* **99**, 022503 (2007).
- [6] A. Ozawa, T. Kobayashi, T. Suzuki, K. Yoshida and I. Tanihata, *Phys. Rev. Lett.* **84**, 5493 (2000).
- [7] K. Tshoo *et al.*, *Phys. Rev. Lett.* **109**, 022501 (2012).
- [8] I. Talmi and I. Unna, *Phys. Rev. Lett.* **4**, 469 (1960).
- [9] T. Otsuka, T. Suzuki, R. Fujimoto, H. Grawe, and Y. Akaishi, *Phys. Rev. Lett.* **95**, 232502 (2005).
- [10] A. P. Zuker, *Phys. Rev. Lett.* **90**, 042502 (2003).
- [11] T. Otsuka *et al.*, *Phys. Rev. Lett.* **104**, 012501 (2010).
- [12] A. Bohr and B.R. Mottelson, *Nuclear Structure*, Vol. 1 (World Scientific, Singapore, 1998).
- [13] A. Huck *et al.*, *Phys. Rev. C* **31**, 2226 (1985).
- [14] R. V. F. Janssens *et al.*, *Phys. Lett. B* **546**, 55 (2002).
- [15] J. I. Prisciandaro *et al.*, *Phys. Lett. B* **510**, 17 (2001).
- [16] D. Steppenbeck *et al.*, *Phys. Rev. Lett.* **114**, 252501 (2015).
- [17] D.-C. Dinca *et al.*, *Phys. Rev. C* **71**, 041302(R) (2005).
- [18] A. Bürger *et al.*, *Phys. Lett. B* **622**, 29 (2005).
- [19] F. Wienholtz *et al.*, *Nature (London)* **498**, 346 (2013).
- [20] M. Rosenbusch *et al.*, *Phys. Rev. Lett.* **114**, 202501 (2015).
- [21] X. Xu *et al.*, *Chin. Phys. C* **39**, 104001 (2015).
- [22] R. F. Garcia Ruiz *et al.* *Nature (London)* **12**, 594 (2016).
- [23] E. Leistenschneider *et al.*, *Phys. Rev. Lett.* **120**, 062503 (2018).
- [24] D. Steppenbeck *et al.*, *Nature (London)* **502**, 207 (2013).
- [25] S. Michimasa *et al.*, *Phys. Rev. Lett.* **121**, 022506 (2018).
- [26] H. Suzuki *et al.*, *Phys. Rev. C* **88**, 024326 (2013).
- [27] S. Zhu *et al.*, *Phys. Rev. C* **74**, 064315 (2006).
- [28] D. Steppenbeck *et al.*, *Phys. Rev. C* **96**, 064310 (2017).
- [29] G. Hagen, M. Hjorth-Jensen, G. R. Jansen, R. Machleidt, and T. Papenbrock, *Phys. Rev. Lett.* **109**, 032502 (2012).
- [30] Y. Utsuno *et al.*, *JPS Conf. Proc.* **6**, 010007 (2015).
- [31] N. Fukuda, T. Kubo, T. Ohnishi, N. Inabe, H. Takeda, D. Kameda, and H. Suzuki, *Nucl. Instrum. Methods Phys. Res., Sect. B* **317**, 323 (2013).
- [32] T. Kubo *et al.*, *Prog. Theor. Exp. Phys.* **2012**, 03C003 (2012).
- [33] T. Kobayashi *et al.*, *Nucl. Instrum. Methods Phys. Res., Sect. B* **317**, 294 (2013).
- [34] A. Obertelli *et al.*, *Eur. Phys. J. A* **50**, 8 (2014).
- [35] C. Santamaria *et al.*, *Nucl. Instrum. Methods Phys. Res., Sect. A* **905**, 138 (2018).
- [36] S. Takeuchi *et al.*, *Nucl. Instrum. Methods Phys. Res., Sect. A* **763**, 596 (2014).
- [37] S. Agostinelli *et al.*, *Nucl. Instrum. Methods Phys. Res., Sect. A* **506**, 250 (2003).
- [38] S. Raman *et al.*, *At. Data Nucl. Data Tables* **78**, 1 (2001).
- [39] M. Wang, G. Audi, F. G. Kondev, W. J. Huang, S. Naimi, and X. Xu, *Chin. Phys. C* **41**, 030003 (2017).
- [40] <http://www.nndc.bnl.gov/>.
- [41] S. -C. Wu, *Nucl. Data Sheets* **91**, 1 (2000).
- [42] K. Tsukiyama, S. K. Bogner, and A. Schwenk, *Phys. Rev. C* **85**, 061304(R) (2012).
- [43] S. R. Stroberg, H. Hergert, J. D. Holt, S. K. Bogner, and A. Schwenk, *Phys. Rev. C* **93**, 051301(R) (2016).
- [44] H. Hergert, S. K. Bogner, T. D. Morris, A. Schwenk, and K. Tsukiyama, *Phys. Rep.* **621**, 165 (2016).
- [45] S. R. Stroberg *et al.*, *Phys. Rev. Lett.* **118**, 032502 (2017).
- [46] J. Simonis, S. R. Stroberg, K. Hebeler, J. D. Holt, and A. Schwenk, *Phys. Rev. C* **96**, 014303 (2017).
- [47] R.J. Bartlett and M. Musiał, *Rev. Mod. Phys.* **79**, 291 (2007).
- [48] G. Hagen, T. Papenbrock, M. Hjorth-Jensen, and D. J.

- Dean, Rep. Prog. Phys. **77**, 096302 (2014).
- [49] E. Epelbaum, H.-W. Hammer, and U.-G. Meiner, Rev. Mod. Phys. **81**, 1773 (2009).
 - [50] R. Machleidt and D. R. Entem, Phys. Rep. **503**, 1 (2011).
 - [51] K. Hebeler, S. K. Bogner, R. J. Furnstahl, A. Nogga, and A. Schwenk, Phys. Rev. C **83**, 031301 (2011).
 - [52] J. Simonis, K. Hebeler, J.D. Holt, J. Menéndez, and A. Schwenk, Phys. Rev. C **93**, 011302(R) (2016).
 - [53] A. Ekström *et al.*, Phys. Rev. C **91**, 051301(R) (2015).
 - [54] G. R. Jansen, M. Hjorth-Jensen, G. Hagen, and T. Papenbrock, Phys. Rev. C **83**, 054306 (2011).
 - [55] John D. Watts and Rodney J. Bartlett, Chemical Physics Letters **258**, 581 (1996).
 - [56] Y. Utsuno, T. Otsuka, B. A. Brown, M. Honma, T. Mizusaki, and N. Shimizu, Phys. Rev. C **86**, 051301(R) (2012).
 - [57] J. Papuga *et al.*, Phys. Rev. Lett. **110**, 172503 (2013).
 - [58] T. Aumann, C. A. Bertulani, and J. Ryckebusch, Phys. Rev. C **88**, 064610 (2013).
 - [59] C. A. Bertulani and C. De Conti, Phys. Rev. C **81**, 064603 (2010).
 - [60] L. Lapikás, Nucl. Phys. A **553**, 297 (1993).
 - [61] L. Atar *et al.*, Phys. Rev. Lett. **120**, 052501 (2018).
 - [62] S. Kawase *et al.*, Prog. Theor. Exp. Phys. **2018**, 021D01 (2018).
 - [63] E. Bitterwolf *et al.*, Z. Physik A **313**, 123 (1983).
 - [64] T. Duguet, H. Hergert, J. D. Holt, and V. Soma, Phys. Rev. C **92**, 034313 (2015).
 - [65] J. D. Holt *et al.* (manuscript in preparation).
 - [66] O. B. Tarasov *et al.*, Phys. Rev. Lett. **121**, 022501 (2018).